

... ..

Verifying pore network models of imbibition in rocks using time-resolved synchrotron imaging

Tom Bultreys^{1,2}, Kamaljit Singh¹, Ali Q. Raeini¹, Leonardo C. Ruspini³, Pål-Eric Øren³,
Steffen Berg⁴, Maja Rücker⁵, Branko Bijeljic¹, Martin J. Blunt¹

¹Department of Earth Science and Engineering, Imperial College London, London, SW7 2AZ, United Kingdom

²UGCT/PProGRes, Dept. of Geology, Ghent University, Belgium

³Petricore Norway AS, Trondheim, Norway

⁴Shell Global Solutions BV, Amsterdam, The Netherlands

⁵Department of Chemical Engineering, Imperial College London, United Kingdom

Key Points:

- A new method to compare pore network simulations of two-phase flow to time-resolved micro-CT data
- Evolution of fluid distributions were validated with respect to pore size, connectivity and flow paths
- Quasi-static pore network models put the fluids in approximately the right pores to predict flow properties

Corresponding author: Tom Bultreys, Tom.Bultreys@UGent.be

Abstract

At the pore scale, slow invasion of a wetting fluid in porous materials is often modelled with quasi-static approximations which only consider capillary forces in the form of simple pore filling rules. The appropriateness of this approximation, often applied in pore network models, is contested in literature, reflecting the difficulty of predicting imbibition relative permeability with these models. However, validation by sole comparison to continuum-scale experiments is prone to induce model overfitting. It has therefore remained unclear whether difficulties generalizing the model performance are due to network extraction, the pore filling rules, or whether a quasi-static description is useful at all. Here, we address this by examining whether such a model can predict the pore-scale fluid distributions underlying the behaviour at the continuum scale. To this end, we compare the fluid arrangement evolution measured in fast synchrotron micro-CT experiments on two rock types to quasi-static simulations which implement capillary-dominated pore filling and snap-off, including a sophisticated model for cooperative pore filling. The results indicate that pore network models with appropriate pore filling rules can in principle obtain a good first-order prediction of the upscaled flow properties of strongly-wetted rocks at low capillary numbers.

1 Introduction

Dunking a biscuit into tea, which then soaks up the liquid, is an everyday example of a wetting fluid (tea) displacing a non-wetting fluid (air) in a porous medium (biscuit). This process, termed imbibition, occurs in nature in the topmost layer of soil during rainfall, during the flow of immiscible pollutants in ground water resources, the geological storage of carbon dioxide or hydrogen, and the management of petroleum reservoirs [Bickle, 2009; Atteia *et al.*, 2013; Blunt, 2017]. To understand the link between pore structure, wettability and upscaled multi-phase flow parameters, a large amount of effort has been put into simulating the pore-scale fluid distribution and calculating the corresponding macroscopic properties [Meakin and Tartakovsky, 2009; Bultreys *et al.*, 2016a].

The key challenge in this field is to describe the intricate arrangement of the two fluids in the pore space during the fluid invasion [Herring *et al.*, 2013; Armstrong *et al.*, 2016; Zhao *et al.*, 2016]. Models struggle to capture the effect of the many fluid-fluid interface movements on the fluid flow over sufficiently large length and time scales [Meakin and Tartakovsky, 2009]. While Navier-Stokes solvers are becoming mature enough to perform useful numerical experiments on domains tens of pores across over relatively short time scales [Fer-

49 *rari and Lunati, 2013; Shams et al., 2018; Alpak et al., 2018; McClure et al., 2018*], it re-
50 mains desirable to define a more conceptual model which describes the emergence of struc-
51 tures at the scale of fluid clusters for upscaling [*Hilfer et al., 2015*].

52 Pore network models (PNMs) conceptualize the pore space as a network of larger void
53 volumes, pores, bounded by restrictions, called throats (Figure 2). In Earth science cases, the
54 global flow rates are typically so low that the capillary force is often assumed to be domi-
55 nant at the pore scale [*Blunt, 2017*]. The most computationally efficient type of pore network
56 models therefore adopts the quasi-static assumption: only capillary forces are taken into ac-
57 count and the fluids are assumed in capillary quasi-equilibrium at each moment [*Wilkinson*
58 *and Willemsen, 1983; Blunt et al., 1992*]. The fluid invasion process is abstracted into filling
59 rules which aim to produce similar emerging fluid distribution patterns as when the capillary,
60 viscous and inertial forces drive the process in reality [*Blunt et al., 2013*]. The pore space is
61 invaded as a sequence of invasion events of three types: snap-off, piston-like displacement
62 and cooperative pore filling [*Lenormand et al., 1983*]. Predicting the evolution of the pore-
63 scale fluid distribution therefore reduces to calculating the entry capillary pressure for each
64 of these events in all available pores, and gradually filling the pore space with the invading
65 fluid in order of this pressure. Dynamic pore network models, on the other hand, explicitly
66 capture the visco-capillary force balance of immiscible transport [*Lenormand et al., 1983;*
67 *Joekar-Niasar and Hassanzadeh, 2012*], but come at the price of increased complexity and
68 computational demands.

69 While a number of early studies have showed that quasi-static PNMs can match exper-
70 imental relative permeability curves in specific cases [*Øren et al., 1998; Valvatne and Blunt,*
71 *2004; Blunt et al., 2013*], substantial efforts over several decades have not led to satisfying
72 predictive capabilities in a general sense [*Bondino et al., 2012*]. It has been unclear whether
73 the shortcomings originate from uncertainties in the extracted network, the pore filling rules,
74 or whether it is adequate to use a quasi-static description at all. Newly available fast time-
75 resolved X-ray micro-CT experiments [*Wildenschild and Sheppard, 2013; Youssef et al.,*
76 *2013; Berg et al., 2013; Andrew et al., 2015; Bultreys et al., 2016b; Schlüter et al., 2017;*
77 *Singh et al., 2017*] have challenged the quasi-static assumption, as viscous and inertial effects
78 such as ganglion dynamics and intermittency have been observed [*Rücker et al., 2015; Arm-*
79 *strong et al., 2016; Gao et al., 2017; Reynolds et al., 2017*]. However, it is currently not well
80 understood how strongly the quasi-static approximation deviates from the experimental real-
81 ity in rock samples, and if this produces fundamentally flawed predictions at the intermediate

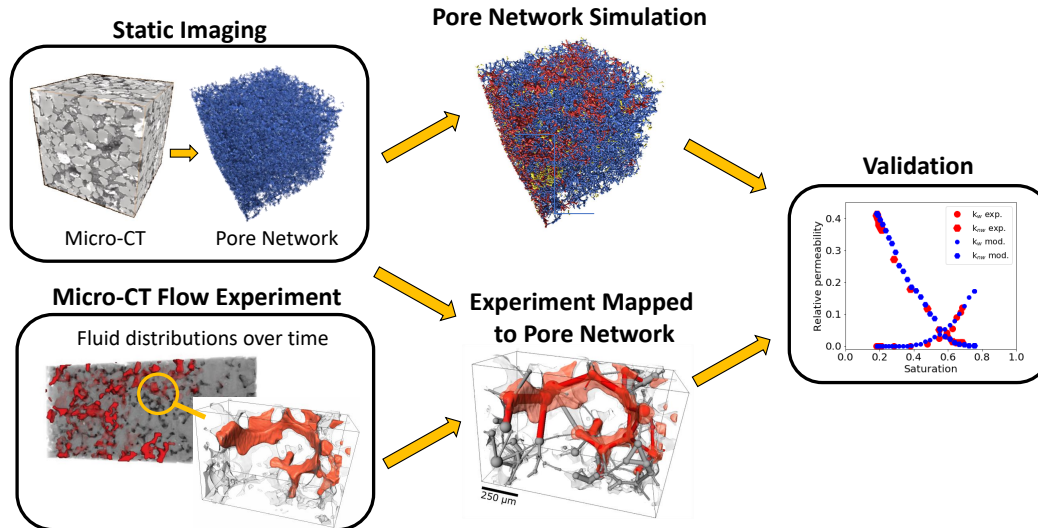
82 scale of the fluid clusters. The validation question is complicated by the fact that model sim-
83 plifications lead to a large number of internal microscopic degrees of freedom, but the output
84 consists of relatively few macroscopic parameters that can be used for validation. Therefore,
85 there is a risk of overfitting the model when tuning it to experimentally measured continuum
86 scale flow properties, e.g. relative permeability and capillary pressure-saturation functions
87 [Bondino *et al.*, 2012; Aghaei and Piri, 2015; Masalmeh *et al.*, 2015; Jerauld *et al.*, 2017].
88 Instead, criteria which contain enough information to reconstruct the relevant aspects of the
89 system’s internal state are required [Liu *et al.*, 2013].

90 In a previous study, we showed how PNM predictions can be mapped to fluid distribu-
91 tions measured with micro-CT to facilitate direct pore-by-pore comparisons [Bultreys *et al.*,
92 2018]. Here, we extend this to time-resolved micro-CT datasets to validate the filling se-
93 quence rather than a static snap-shot, resulting in a more complete picture. The experimental
94 data in this study are two publicly available fast synchrotron micro-CT datasets of water-
95 flooding in strongly water-wet Ketton limestone [Singh *et al.*, 2017] and Gildehauser sand-
96 stone [Rücker *et al.*, 2015]. This study investigates whether a quasi-static assumption can
97 result in realistic filling sequences for strong imbibition at low capillary numbers. Contrary
98 to previous studies, e.g. Berg *et al.* [2016], the models used here implement snap-off and
99 cooperative pore filling processes on experimentally based geometries [Valvatne and Blunt,
100 2004; Ruspini *et al.*, 2017]. We used a realistic cooperative pore filling algorithm [Ruspini
101 *et al.*, 2017], and minimized the influence of the specific PNM extraction and of the bound-
102 ary conditions on the analysis. The general workflow is depicted in figure 1. We find that
103 the quasi-static model generally puts the fluids in the right pores to approximate mm-scale
104 averaged properties, at least in strongly water-wet samples at low capillary numbers.

110 2 Materials and methods

111 2.1 Experiments

112 Details of the Ketton and Gildehauser unsteady-state (constant injection flow rate)
113 imbibition experiments are described in Singh *et al.* [2017] and Rücker *et al.* [2015]. Both
114 datasets are publicly available [Singh *et al.*, 2018; Berg *et al.*, 2018]. Ketton and Gildehauser
115 (the latter a local variety of Bentheimer) respectively have a porosity of 23 % and 20 %; and
116 a permeability of $2.8 \times 10^{-12} \text{ m}^2$ and $1.48 \times 10^{-12} \text{ m}^2$ [Andrew *et al.*, 2014]. In the experi-
117 ments, KI-brine was used as the wetting phase and decane as the non-wetting phase. As the



105 **Figure 1.** The workflow for validation of pore scale multi-phase flow models proposed in this paper. After
 106 extracting a pore network model from a micro-CT scan of the sample, we generated a series of fluid distribu-
 107 tions in the pore network model by either numerical simulation or experimental micro-CT imaging. We then
 108 investigate whether the simulation succeeds at filling pores in approximately the right order compared to the
 109 experiment, particularly with regards to predicting upscaled flow properties.

118 samples were clean quarry stones, they were water-wet. Cylindrical samples with a diame-
 119 ter of approximately 4 mm and a height of 10 mm were inserted into flow cells. First, a high
 120 quality dry micro-CT scan was obtained. Next, the samples were fully saturated with brine
 121 and drained by injecting decane. Then, imbibition was initiated by injecting brine at very
 122 low capillary numbers (1.26×10^{-9} in the Ketton case, 1.8×10^{-8} in the Gildehauser case).
 123 During imbibition, each sample was partly imaged along its height by fast micro-CT (Ketton:
 124 400 scans at 38 seconds/scan, voxel size $3.28 \mu\text{m}$, image height 3.28 mm; Gildehauser: 40
 125 scans at 45 seconds/scan, voxel size $4.4 \mu\text{m}$, image height 2.49 mm). Imaging was performed
 126 at I13-2 (Diamond Light Source) and at TOMCAT (Swiss Light Source). As detailed in the
 127 aforementioned references, the images were treated with a non-local means filter and seg-
 128 mented with the watershed algorithm in Avizo 9 (ThermoFisher/FEI). The final Gildehauser
 129 image contained an oil cluster connected to the top and the bottom of the image, i.e. the oil
 130 in the sample may still have been mobile.

2.2 Quasi-static modelling

The pore network models used here were extracted from the segmented dry scans using the maximal ball method [Raeini *et al.*, 2017]. This method employs the distance map of the pore space image to find pores and throats as constrictions and dilations. The radii of these elements were found by looking for the maximum inscribed spheres at these locations. Shape factors were used to describe the angularity of pores and throats as described in *Bultreys et al.* [2018]. The pores and throats had circular, triangular and square cross-sections, based on their shape factor [Valvatne and Blunt, 2004].

After network extraction, imbibition was simulated using a quasi-static invasion percolation approach, based on *Øren et al.* [1998], *Valvatne and Blunt* [2004] and *Ruspini et al.* [2017]. Following these works, entry pressures were calculated for each pore and throat which could be accessed by the invading fluid and from which the defending fluid had an escape path (i.e. was not trapped). The pressure calculations are summarized in the Supporting Information. The wetting phase was injected from the top and bottom face, and the non-wetting phase was allowed to escape through both, to account for backflow in the porous medium outside the field of view. We used the fluid occupancy at the start of imbibition in the experimental data to assign the initial condition of the model. Advancing contact angles were randomly assigned to each pore or throat in the range between 35 and 45 degrees for Ketton [Scanziani *et al.*, 2017] and 35 and 55 degrees for Gildehauser [Khishvand *et al.*, 2016], based on in situ contact angle measurements. We list here the PNM assumptions and parameters which can influence the simulated filling sequence:

- The segmentation of the micro-CT scan. While this can have an important effect on the network extraction and simulations, the large pores and the good image quality in the dry scans was deemed to lead to high quality segmentations. We used the segmented images provided in the public domain data sets, without tuning the segmentation to improve the PNM results.
- The detection of pore and throat centres as local minima and maxima of the distance map. The main user-defined parameter is the minimum inscribed radius for a point to be called a pore centre, set to 1.5 voxel lengths. This does not affect the results for the well-resolved, rather simple pore structures in this work. In any event, the same network extraction was used to analyse both the experiment and the model.

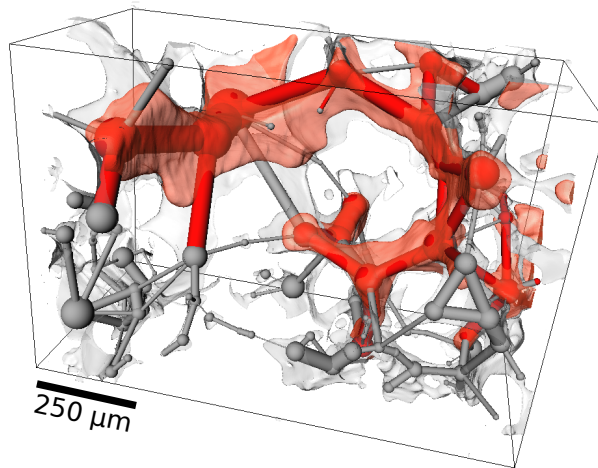
- 162 • Pore and throat shape factor determination, and the simplification of pore shapes to
163 (predominantly) triangles with the same shape factor and inscribed radius [*Øren et al.*,
164 1998]. This induces an approximation, but it is fully defined by the detection of pore
165 centres and throat surfaces.
- 166 • Advancing contact angle assignment. These were randomly assigned in each pore or
167 throat in the range between 35 degrees and 45 degrees for Ketton [*Singh et al.*, 2016;
168 *Scanziani et al.*, 2017] and 35 degrees and 55 degrees for Gildehauser [*Khishvand*
169 *et al.*, 2016], based on in situ contact angle measurements. The sensitivity within
170 likely values (several ranges spanning 25 degrees to 65 degrees) was found not to in-
171 fluence the conclusions in this paper, as shown in the Supporting Information.
- 172 • The capillary pressure reached during drainage, prior to imbibition. This is inferred
173 from the radius of the smallest pore or throat that is oil-filled in the micro-CT image
174 after drainage.
- 175 • One parameter in the cooperative pore filling algorithm, which determines when the
176 interface becomes unstable while entering the throats. This parameter has a very lim-
177 ited influence on the simulations results [*Ruspini et al.*, 2017].

178 **2.3 Data analysis**

179 To allow consistent comparison of the experiments to PNM simulations, we used the
180 PNM as an image analysis tool on the imbibition datasets. As detailed in *Bultreys et al.*
181 [2018], the inscribed spheres at each pore and throat centre in the dry scan were determined
182 during network extraction. These were used to define the fluid occupying the pore or throat
183 centre. For each time step in the imbibition experiment, a pore or throat was called wetting-
184 filled if more than half of the voxels of the associated inscribed sphere are segmented as wet-
185 ting fluid. The simulations were run on the same PNM used to analyse the experiments, en-
186 abling a like-for-like comparison (Figure 2). The measures shown in this paper were calcu-
187 lated on the PNM structure, with fluid distributions mapped from the experiments, or from
188 simulations on the PNM.

194 **2.3.1 Filling size**

195 Pores and throats in the experiment were considered to be invaded at time step t if they
196 were filled with wetting fluid in image t and with non-wetting fluid in image $t - 1$. If they



189 **Figure 2.** Voids in Ketton limestone, with the non-wetting fluid observed in one of several hundred snap-
 190 shots of an imbibition experiment indicated in transparent red (the figure shows a small subvolume of a
 191 micro-CT scan). The balls and sticks represents the corresponding pore network model, colored according
 192 to the fluids occupying each pore or throat in a simplified model of fluid invasion. We use this one-to-one
 193 mapping to compare the evolving fluid filling pattern to the experiment.

197 changed filling state more than 3 times, they were not listed here, as these were a small num-
 198 ber of mainly narrow throats affected by image noise. The filling time was then translated to
 199 the filling sequence rank number (the rank of the pore or throat filling event when ordered
 200 according to the filling time). This was necessary because the simulations do not have a time
 201 scale, but only predict in which order pores and throats fill. In the Gildehauser case, the rate
 202 of filling was relatively large compared to the time resolution of the imaging. Therefore, fill-
 203 ing sizes at certain time steps in this experiment are shown using box plots with outliers.

204 **2.3.2 Connectivity**

205 To characterize the connectivity, we calculate the Euler characteristic of the shape
 206 formed by the throats (conceptualized here as cylinders) and pores (conceptualized as spheres)
 207 that are filled with the non-wetting phase from either the experiment or the simulation. We
 208 first remove isolated non-wetting phase-filled throats to reduce the dependency on imaging
 209 noise. Then, we modify this shape by adding a sphere to the end of any cylinder which does
 210 not already end in a sphere. This does not change the Euler characteristic as it is invariant
 211 under continuous deformation of the shape. The Euler characteristic χ can be calculated us-

212 ing the Betti numbers β_i :

$$\chi = \beta_0 - \beta_1 + \beta_2 \tag{1}$$

213 Here, β_0 equals the number of connected components k and β_2 is the number of holes
 214 in the shape, the latter by construction equaling zero. β_1 is the number of loops in the shape
 215 [Wildenschild and Sheppard, 2013], equalling $N_e - N_v + k$, with N_e the number of edges and
 216 N_v , the number of vertices of the corresponding graph [Berge, 2001]. Therefore, the calcula-
 217 tion of the Euler characteristic reduces to:

$$\chi = N_v - N_e \tag{2}$$

218 Note that the calculation does not depend on the exact pore and throat shapes. Detect-
 219 ing the connected components in the non-wetting phase graph allows to calculate the amount
 220 and sizes of clusters, after which the amount of loops can be calculated as $k - \chi$.

221 **2.3.3 Flow paths**

222 The relevance of discrepancies in the filling sequence to relative permeabilities is a
 223 question of key concern [Berg *et al.*, 2016]. However, the calculation of volumes and fluid
 224 flow conductances for each pore and throat induces non-uniqueness associated with user-
 225 defined parameters [Sorbie and Skauge, 2011]. Since we are only interested here in the fluid
 226 displacements and not in improving conductivity or saturation calculations, we circumvent
 227 this problem by calculating relative permeabilities for both the experimental and the simu-
 228 lated fluid distributions on the same PNM, using the same (possibly imprecise) conductivi-
 229 ties and volumes. This yields a flow-weighted connectivity metric which is a proxy to (but
 230 not necessarily equal to) physical relative permeability measurements.

231 For the experiments, relative permeabilities were calculated by mapping the experi-
 232 mentally observed fluid distribution on the same PNM as used in the imbibition simulations.
 233 The Hagen-Poiseuille conductivity model was used to calculate the flow rates through the
 234 wetting and the non-wetting phase separately, using the OpenPNM pore network modelling
 235 package [Gostick *et al.*, 2016]. We assumed that throats filled with one phase have zero con-
 236 ductivity for the other phase. Flow rates for the simulations were calculated on the same
 237 PNM with the same conductivities, and discrepancies compared to the experiment therefore
 238 came solely from differences in the fluid distribution. A good match means the flow distri-
 239 bution in the model is approximately correct to predict the upscaled properties. However, to

240 match experimentally measured relative permeabilities (based on pressure measurements),
241 it may still be necessary to improve the volume and conductivity assignment of pores and
242 throats. This less fundamental issue is outside the scope of the study.

243 **Results and discussion**

244 Previous studies have shown that the pore-scale fluid distribution in experiments is not
245 fully reproducible [Ferrari *et al.*, 2015; Ling *et al.*, 2017; Bultreys *et al.*, 2018]. The averaged
246 properties are, however, much more reproducible, as different realisations of the fluid distri-
247 bution can lead to consistent averaged results if they are statistically similar. Therefore, sim-
248 ply comparing the filling sequence on a pore-by-pore basis does not offer a relevant answer
249 [Bultreys *et al.*, 2018]. Recognizing that a good prediction of the upscaled multi-phase flow
250 properties needs to capture the geometry and the connectivity of the fluid phases throughout
251 the filling sequence, we use the following criteria to validate the model:

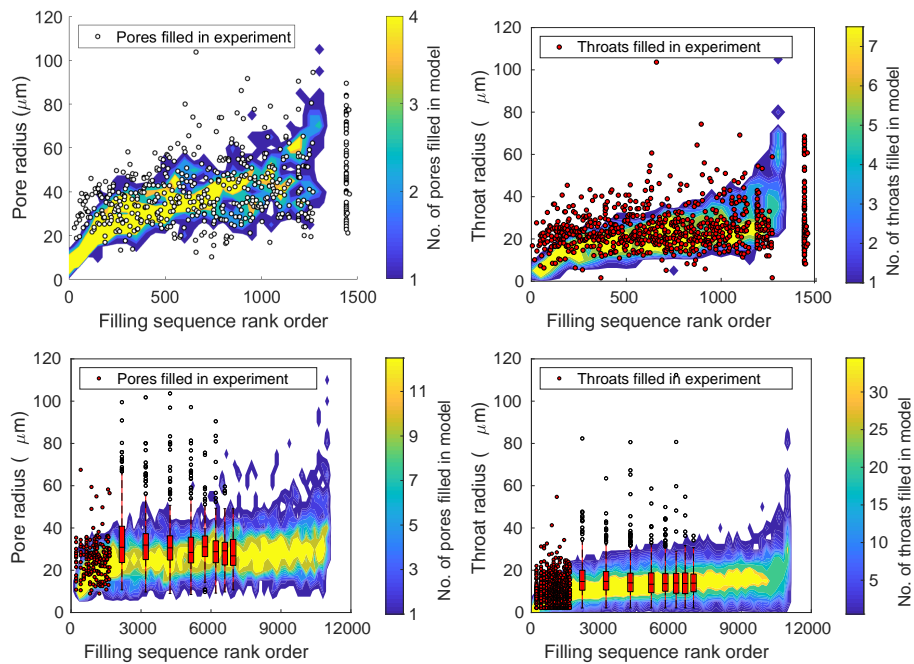
- 252 • In terms of size (radius), which pores and throats are filled throughout the filling se-
253 quence?
- 254 • How does the connectivity of the non-wetting phase change during the filling se-
255 quence?
- 256 • How do the flow paths of the wetting and the non-wetting phase change throughout
257 the filling sequence?

258 As our goal was to evaluate physical concepts rather than model implementation, the
259 influence of PNM non-uniqueness on the validation was reduced as much as possible. Pa-
260 rameters that affect the filling sequence were set based on physical principles and were sensitivity-
261 checked.

262 **Filling size**

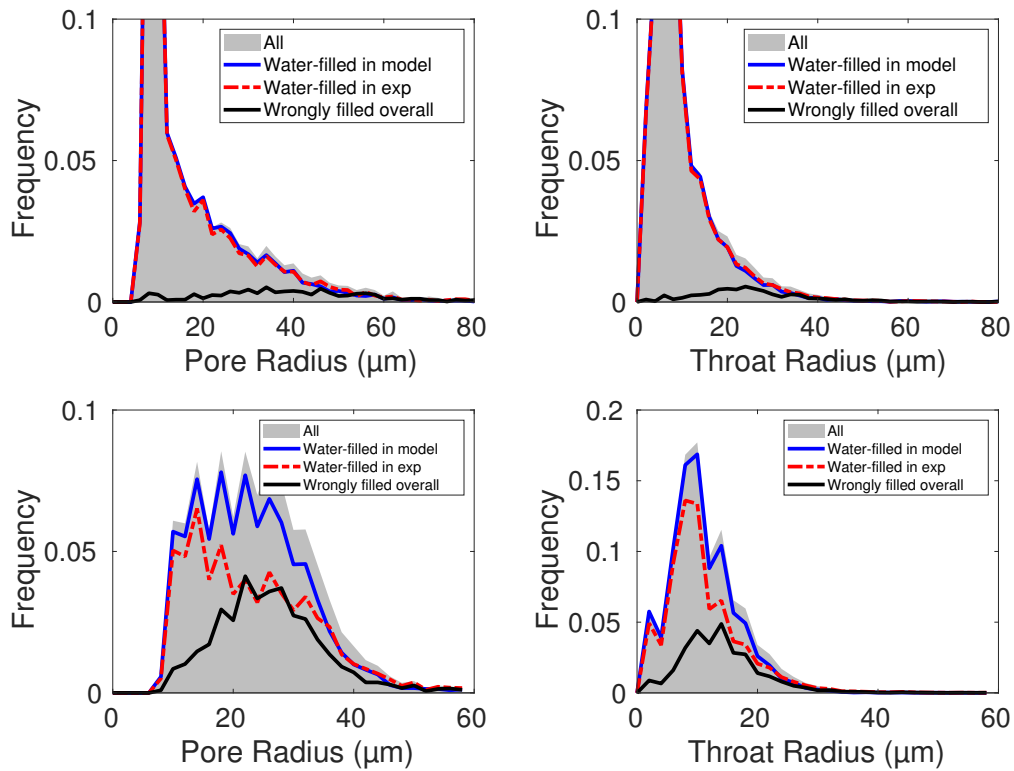
263 The PNM used in this study explicitly defines pores as local dilations and throats as
264 local constrictions [Raeini *et al.*, 2017]. In terms of the associated capillary energy, pores
265 should locally be less favourable places for the invading wetting phase to pervade, while
266 throats should be more favourable. Therefore, we tracked the invasion of the wetting phase
267 in these locations in the experiment and the model, using the same network extraction on
268 both. We define filling in the experiment as events where the image shows a change in oc-

269 cupancy, such that the voxels associated with the maximal sphere centred on a pore or throat
 270 first become occupied principally by the wetting phase in the segmented image.



271 **Figure 3.** Pore and throat filling sizes in the the model and the experiment for Ketton (top row) and Gilde-
 272 hauser (bottom row) matched well, although there is a tendency for a small number of larger elements to be
 273 filled in the experiment and not by the model. Dots and box plots (for time steps where many network ele-
 274 ments were invaded at the same time) present the radii of pores and throats filled with the invading wetting
 275 phase during the experiment in rank order. The contour plots show the pore or throat radii filled in the model.

276 Figure 3 shows the radii of pores and throats that were invaded during the experiment
 277 as a function of their rank order in the filling sequence. In general, pores and throats of simi-
 278 lar sizes were filled throughout the filling sequence in the experiment and the model. In both
 279 cases, filling did not strictly happen in order of increasing radius due to the occurrence of the
 280 three types of filling (snap-off, piston-like advance and cooperative pore filling) and the vari-
 281 ation in pore and throat shapes. A small number of pores and throats with large radii were
 282 filled in the experiment, but not in the simulations. This could be related to geometry simpli-
 283 fications in the network model, to local variations in wettability [AlRatrou et al., 2018], or
 284 to viscous and/or inertial effects which are not captured in the quasi-static PNM. A decrease
 285 of the local capillary pressure caused by the latter two effects may have led to the invasion of
 286 pores with larger characteristic size than predicted by the quasi-static model.



287 **Figure 4.** Pore and throat sizes that are filled with water at the end of imbibition, for Ketton (top row) and
 288 Gildehauser (bottom row). The black line indicates the frequency of pore and throat sizes that were filled with
 289 fluid in the model different than in the experiment.

290 Figure 4 shows the size distribution of the water-filled pores and throats in the experi-
291 ments and the model after imbibition, and indicates pores and throats filled with a fluid in the
292 model different from the experiment, similar to *Bultreys et al.* [2018] and *Øren et al.* [2019].
293 In the Ketton experiment both model and experiment reached residual saturation. There is
294 a very close agreement, with a filling discrepancy of 9 % in the pores and 6 % in the throats
295 (the percentage of pores or throats that were filled with a different fluid in the model as in the
296 experiment).

297 The Gildehauser experiment did not reach the residual saturation in the experimen-
298 tal field of view, and therefore we compared the simulated fluid distribution with the same
299 saturation as the final state in the experiment. The model overpredicted the number of water-
300 filled pores and throats, resulting in a filling discrepancy of 30 % in the throats and 38 % in
301 the pores. This is explained by the fact that the simulation was stopped at the same saturation
302 as the experiment, while a number of large pores were filled earlier in the experiment than
303 in the model (Figure 3). A previous study showed filling discrepancies of 18 % and 21 % for
304 PNM simulations compared to steady-state Bentheimer experiments at the end of imbibition
305 [*Bultreys et al.*, 2018], and a standard deviation of up to 25 % on the pore occupancy for the
306 intermediately-sized pores in repeated experiments. A different study on Paaratte sandstone
307 found filling discrepancies of 15 % and 13 % [*Øren et al.*, 2019].

308 The validation of pore and throat filling sizes presented here improves on the approach
309 in *Bultreys et al.* [2018] and *Øren et al.* [2019] because it took the dynamics of the filling
310 process into account. Overall, a more favourable agreement was found here than in *Bultreys*
311 *et al.* [2018] due to the use of a different cooperative pore filling algorithm [*Ruspini et al.*,
312 2017] and initial and boundary conditions that more closely resembled those of the experi-
313 ment. The cooperative pore filling algorithm developed by *Ruspini et al.* [2017] is a signifi-
314 cant improvement over the previously available algorithms because it accounts for the local
315 geometry of the surrounding throats to assign the capillary invasion pressures.

316 In repeated drainage-imbibition experiments on Bentheimer, the standard deviation of
317 the filling state was found to be up to 25 % for the most variable pores, while the large-scale
318 behaviour did not vary significantly [*Bultreys et al.*, 2018]. The filling discrepancy between
319 the PNM simulation and the experiment is thus of similar magnitude to the difference be-
320 tween two repeat experiments that are macroscopically nearly indistinguishable.

Connectivity

The upscaled flow characteristics are strongly influenced by the phase connectivity [Hilfer, 2006], which can be characterized by the Euler characteristic [Armstrong *et al.*, 2016; Schlüter *et al.*, 2016]. We compared the evolution of the Euler characteristic during imbibition in the model and the experiment (Figure 5). A consistent comparison to the simulations was achieved by mapping the experimental distributions on the PNM and calculating the Euler characteristic there. The experimental trend is consistent with direct image-based calculations [Alpak *et al.*, 2018].

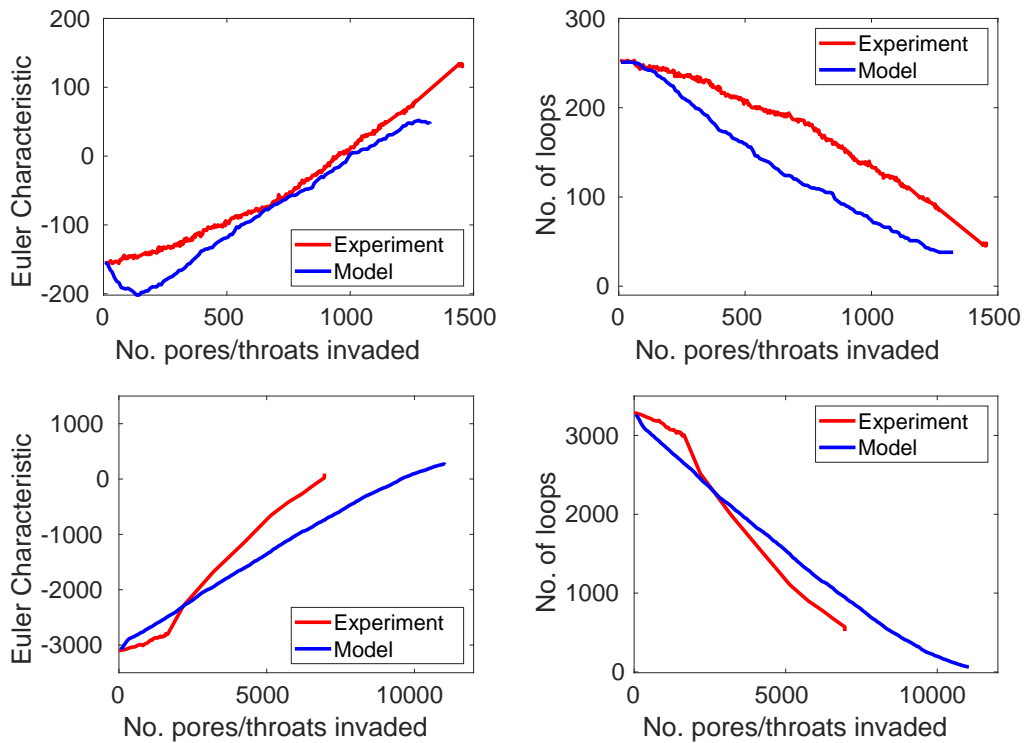


Figure 5. Comparison of the evolution of the non-wetting phase Euler characteristic in the experiment and in the model (left) and the amount of loops in the non-wetting phase (right), for Ketton (top) and Gildehauser (bottom). A large negative Euler characteristic indicates that the non-wetting phase is well connected with many loops in the structure.

Figure 5 shows that magnitude and trends of the Euler characteristic are correctly represented by the model. There are, however, some discrepancies. In the Ketton simulation the model shows a local minimum at the start of imbibition. This is caused by an image processing artifact: small pores that were wrongly identified as non-wetting-filled after drainage.

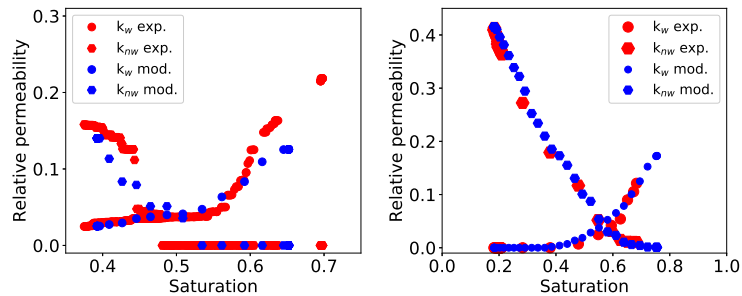
337 The effect of this on the Euler characteristic was partly compensated by redundant loops in
338 the modelled non-wetting phase distribution being removed too quickly. The latter may have
339 been caused by a mismatch in the amount of cooperative pore filling compared to snap-off
340 between the simulation and the experiment, due to geometric simplifications in the model.
341 Imbibition in Ketton is more sensitive to cooperative pore filling than most other rock sam-
342 ples, due to Ketton's pore structure resembling that of a bead pack [Ruspini *et al.*, 2017]. In
343 this particular case, the model may therefore overestimate the amount of capillary trapping.

344 In the Gildehauser case, the Euler characteristic increased more quickly in the experi-
345 ment than in the model. In the experiment, there was a change in the slope of the Euler char-
346 acteristic and the number of loops after approximately 1600 pores and throats were filled.
347 This was likely related to the occurrence of two different filling regimes observed by *Rücker*
348 *et al.* [2015]: first pathway flow and film swelling, and then a regime which includes clus-
349 ter dynamics. This was not reproduced in the model. Furthermore, the faster increase in the
350 experimental Euler characteristic is partly due to misidentification of the fluid occupancy in
351 smaller pores and throats caused by imaging noise in the Gildehauser experiment. This re-
352 sulted in an excessive amount of small non-wetting phase clusters being detected. However,
353 the average sizes of multi-throat clusters (excluding single-throat clusters to reduce imaging
354 noise) were in fair agreement between the model and the experiment, as were the sizes of the
355 largest non-wetting phase clusters which dominate the flow (see Supporting Information). As
356 will be shown in the next section, the discrepancies discussed here had a limited influence on
357 the flow paths through each fluid.

358 **Flow paths**

359 The filled pore/throat sizes and the connectivity together control the flow paths which
360 are accessible to each fluid, and consequently the relative permeability. We compared the
361 flow paths in the model and the experiment by calculating relative permeabilities on the im-
362 aged and the modelled fluid distributions. This relative permeability can be seen as a flow-
363 weighted connectivity of the fluid distributions. Since both the experimental and the mod-
364 elled results used the same conductivity and volume assignments in pores and throats, mis-
365 matches in the presented relative permeabilities can only come from discrepancies in the
366 modelled fluid distributions.

367 The resulting relative permeabilities indicated a close match between the model and
 368 the experiment (Figure 6). This implies that the quasi-static model provided a good estima-
 369 tion of the fluid distribution with respect to its impact on the upscaled flow properties. There
 370 were some discrepancies near the end of imbibition in Ketton. This was likely related to a
 371 small mismatch of cooperative pore filling versus snap-off, and to the boundary conditions,
 372 which were unknown in the experiment due to the limited field of view of the scan. While
 373 ganglion dynamics have been seen to play an important role near the residual non-wetting
 374 phase saturation in the Gildehauser experiment [Rücker *et al.*, 2015], there is no direct evi-
 375 dence of this in the Ketton dataset. We do not draw conclusions about the behaviour near the
 376 end point of imbibition in the Gildehauser case here, as the experiment did not continue until
 377 residual non-wetting saturation.



378 **Figure 6.** Imbibition relative permeability calculations based on the modelled and the experimental fluid
 379 distributions for Ketton (left) and Gildehauser (right) allow to consistently compare the flow paths in the
 380 model and the experiment and indicate a good match.

381 Conclusions

382 A key question concerning imbibition in permeable materials is how to formulate con-
 383 ceptual models that decrease the degrees of freedom compared to an explicit description,
 384 while still capturing the salient behaviour of the process. Quasi-static PNMs abstract the pro-
 385 cess by simplifying the local pore shapes and by assuming that capillary forces are dominant,
 386 allowing imbibition to be described as a sequence of simple pore and throat filling processes.
 387 However, one of the main problems has been validation: the complex relation between the
 388 fluid occupancy of the system and the experimentally measured properties (e.g. relative per-
 389 meability) typically used for validation makes it difficult to understand the origin and gener-

390 ality of any observed (mis-)match [*Sorbie and Skauge, 2011; Bondino et al., 2012; Bultreys*
391 *et al., 2018*].

392 The analysis we have developed here allowed the comparison of pore-scale experimen-
393 tal data to a quasi-static PNM with minimal influence from anything but the fluid distribu-
394 tions. This indicated that the quasi-static assumption provided a good approximation of the
395 order in which pores with different sizes were invaded. The model did misinterpret the filling
396 behaviour of some larger pores, and overestimated the amount of loop-breaking in the non-
397 wetting phase. However, the pores and throats causing these discrepancies showed to be of
398 minor importance for the flow paths, which closely matched the experiments.

399 The conclusion is that an abstracted, conceptually simple model based on quasi-static
400 physics *can* give a good first order approximation of continuum scale properties such as rel-
401 ative permeability, at least in strongly-wetted rocks with relatively homogeneous pore struc-
402 tures and at low capillary numbers. Whether or not it *does*, depends on model implementa-
403 tion (e.g. volume and conductivity assignment) and accurate input concerning pore geometry
404 and advancing contact angles. These less fundamental considerations are outside the scope
405 of this study.

406 In summary, PNMs as a concept appear a valuable starting point for building concep-
407 tual models. However, it must be stressed that more validation needs to point out whether
408 this holds in circumstances where more influence of ganglion dynamics has been observed
409 or can be expected, e.g. near the end of imbibition [*Rücker et al., 2015*], in intermediate /
410 mixed-wet samples [*Zou et al., 2018*] and in samples with very wide pore size distributions.

411 **Acknowledgements**

412 Shehadeh Masalmeh and Ove Bjørn Wilson (Shell) are gratefully acknowledged for
413 pointing out the need for this work and putting us on the right path to executing it. Apos-
414 tolos Georgiadis, Matthias Appel, Xudong Jing and Justin Freeman (Shell) are thanked for
415 valuable discussions on this work. Shell is acknowledged for financial support through the
416 Digital Rocks Programme at Imperial College London, and for permission to publish this pa-
417 per. Tom Bultreys is currently a postdoctoral fellow of the Research Foundation - Flanders
418 (FWO) and acknowledges its support under grant 12X0919N.

419 **References**

420 Aghaei, A., and M. Piri (2015), Direct pore-to-core up-scaling of displacement processes:
 421 Dynamic pore network modeling and experimentation, *Journal of Hydrology*, 522, 488–
 422 509, doi:10.1016/j.jhydrol.2015.01.004.

423 AlRatrouf, A., S. Berg, and I. Zacharoudiou (2018), Prediction of Fluid Topology and Relative
 424 Permeability in Imbibition in Sandstone Rock by Direct Numerical Simulation, *Advances
 425 in Water Resources*, (June), doi:10.1016/j.advwatres.2018.09.001.

426 AlRatrouf, A., M. J. Blunt, and B. Bijeljic (2018), Wettability in complex porous materials,
 427 the mixed-wet state, and its relationship to surface roughness, *Proceedings of the National
 428 Academy of Sciences*, 115(36), 8901–8906, doi:10.1073/pnas.1803734115.

429 Andrew, M., B. Bijeljic, and M. J. Blunt (2014), Pore-scale contact angle measurements at
 430 reservoir conditions using X-ray microtomography, *Advances in Water Resources*, 68, 24–
 431 31, doi:10.1016/j.advwatres.2014.02.014.

432 Andrew, M., H. Menke, M. J. Blunt, and B. Bijeljic (2015), The Imaging of Dynamic Multi-
 433 phase Fluid Flow Using Synchrotron-Based X-ray Microtomography at Reservoir Condi-
 434 tions, *Transport in Porous Media*, 110(1), 1–24, doi:10.1007/s11242-015-0553-2.

435 Armstrong, R. T., J. E. McClure, M. A. Berrill, M. Rücker, S. Schlüter, and S. Berg (2016),
 436 Beyond Darcy’s law: The role of phase topology and ganglion dynamics for two-fluid
 437 flow, *Physical Review E*, 94(043113), doi:10.1103/PhysRevE.94.043113.

438 Atteia, O., E. Del Campo Estrada, and H. Bertin (2013), Soil flushing: a review of the origin
 439 of efficiency variability, *Reviews in Environmental Science and Bio/Technology*, 12(4),
 440 379–389, doi:10.1007/s11157-013-9316-0.

441 Berg, S., H. Ott, S. a. Klapp, A. Schwing, R. Neiteler, N. Brussee, A. Makurat, L. Leu,
 442 F. Enzmann, J.-O. Schwarz, M. Kersten, S. Irvine, and M. Stampanoni (2013), Real-time
 443 3D imaging of Haines jumps in porous media flow, *Proceedings of the National Academy
 444 of Sciences*, 110(10), 3755–3759, doi:10.1073/pnas.1221373110.

445 Berg, S., M. Rücker, H. Ott, A. Georgiadis, H. van der Linde, F. Enzmann, M. Kersten,
 446 R. Armstrong, S. de With, J. Becker, and A. Wiegmann (2016), Connected pathway rel-
 447 ative permeability from pore-scale imaging of imbibition, *Advances in Water Resources*,
 448 90, 24–35, doi:10.1016/j.advwatres.2016.01.010.

449 Berg, S., R. Armstrong, and A. Wiegmann (2018), Micro-CT scans of a fast synchrotron-
 450 based micro-CT flow experiment performed in Gildehauser sandstone rock., doi:
 451 10.17612/P7WW95.

452 Berge, C. (2001), *The theory of graphs*, Courier Dover Publications.

453 Bickle, M. J. (2009), Geological carbon storage, *Nature Geoscience*, 2, 815–818, doi:
 454 10.1038/ngeo687.

455 Blunt, M., M. King, and H. Scher (1992), Simulation and theory of two-phase flow in porous
 456 media, *Physical Review A*, 46(12), 7680–7699, doi:10.1103/PhysRevA.46.7680.

457 Blunt, M. J. (2017), *Multiphase Flow in Permeable Media: A Pore-Scale Perspective*, Cam-
 458 bridge University Press, Cambridge, UK.

459 Blunt, M. J., B. Bijeljic, H. Dong, O. Gharbi, S. Iglauer, P. Mostaghimi, A. Paluszny, and
 460 C. Pentland (2013), Pore-scale imaging and modelling, *Advances in Water Resources*, 51,
 461 197–216, doi:10.1016/j.advwatres.2012.03.003.

462 Bondino, I., G. Hamon, W. Kallel, and D. Kachuma (2012), Relative permeabilities from
 463 simulation in 3D rock models and equivalent pore networks: critical review and way for-
 464 ward, in *Int. Symp. Soc. Core Analysts*, Society for Core Analysts, Society of Core Ana-
 465 lysts, Aberdeen, Scotland.

466 Bultreys, T., W. De Boever, and V. Cnudde (2016a), Imaging and image-based fluid transport
 467 modeling at the pore scale in geological materials: A practical introduction to the current
 468 state-of-the-art, *Earth-Science Reviews*, 155, 93–128, doi:10.1016/j.earscirev.2016.02.001.

469 Bultreys, T., M. N. M. A. Boone, M. N. M. A. Boone, T. De Schryver, B. Masschaele, L. Van
 470 Hoorebeke, and V. Cnudde (2016b), Fast laboratory-based micro-computed tomography
 471 for pore-scale research: Illustrative experiments and perspectives on the future, *Advances*
 472 *in Water Resources*, 95, 341–351, doi:10.1016/j.advwatres.2015.05.012.

473 Bultreys, T., Q. Lin, Y. Gao, A. Q. Raeni, A. AlRatrou, B. Bijeljic, and M. J. Blunt (2018),
 474 Validation of model predictions of pore-scale fluid distributions during two-phase flow,
 475 *Physical Review E*, 97(5), 053,104, doi:10.1103/PhysRevE.97.053104.

476 Ferrari, A., and I. Lunati (2013), Direct numerical simulations of interface dynamics to link
 477 capillary pressure and total surface energy, *Advances in Water Resources*, 57, 19–31, doi:
 478 10.1016/j.advwatres.2013.03.005.

479 Ferrari, A., J. Jimenez-Martinez, T. L. Borgne, Y. Méheust, and I. Lunati (2015), Chal-
 480 lenges in modeling unstable two-phase flow experiments in porous micromodels, *Water*
 481 *Resources Research*, 51(3), 1381–1400, doi:10.1002/2014WR016384.

482 Gao, Y., Q. Lin, B. Bijeljic, and M. J. Blunt (2017), X-ray Microtomography of Intermittency
 483 in Multiphase Flow at Steady State Using a Differential Imaging Method, *Water Resources*
 484 *Research*, 53(12), 10,274–10,292, doi:10.1002/2017WR021736.

- 485 Gostick, J., M. Aghighi, J. Hinebaugh, T. Tranter, M. A. Hoeh, H. Day, B. Spellacy, M. H.
486 Sharqawy, A. Bazylak, A. Burns, W. Lehnert, and A. Putz (2016), OpenPNM: A Pore
487 Network Modeling Package, *Computing in Science & Engineering*, 18(4), 60–74, doi:
488 10.1109/MCSE.2016.49.
- 489 Herring, A. L., E. J. Harper, L. Andersson, A. Sheppard, B. K. Bay, and D. Wilden-
490 schild (2013), Effect of fluid topology on residual nonwetting phase trapping: Impli-
491 cations for geologic CO₂ sequestration, *Advances in Water Resources*, 62, 47–58, doi:
492 10.1016/j.advwatres.2013.09.015.
- 493 Hilfer, R. (2006), Macroscopic capillarity and hysteresis for flow in porous media, *Physical*
494 *Review E*, 73(016307), doi:10.1103/PhysRevE.73.016307.
- 495 Hilfer, R., R. T. Armstrong, S. Berg, A. Georgiadis, and H. Ott (2015), Capillary satura-
496 tion and desaturation, *Physical Review E - Statistical, Nonlinear, and Soft Matter Physics*,
497 92(6), 1–11, doi:10.1103/PhysRevE.92.063023.
- 498 Jerauld, G. R., J. Fredrich, N. Lane, Q. Sheng, B. Crouse, D. M. Freed, A. Fager, and R. Xu
499 (2017), Validation of a Workflow for Digitally Measuring Relative Permeability, *SPE Abu*
500 *Dhabi International Petroleum Exhibition & Conference*, doi:10.2118/188688-MS.
- 501 Joekar-Niasar, V., and S. M. Hassanizadeh (2012), Analysis of Fundamentals of Two-
502 Phase Flow in Porous Media Using Dynamic Pore-Network Models: A Review, *Criti-*
503 *cal Reviews in Environmental Science and Technology*, 42(18), 1895–1976, doi:
504 10.1080/10643389.2011.574101.
- 505 Khishvand, M., M. Akbarabadi, and M. Piri (2016), Micro-scale experimental investigation
506 of the effect of flow rate on trapping in sandstone and carbonate rock samples, *Advances in*
507 *Water Resources*, 94, 379–399, doi:10.1016/j.advwatres.2016.05.012.
- 508 Lenormand, R., C. Zarcone, and A. Sarr (1983), Mechanisms of the displacement of one
509 fluid by another in a network of capillary ducts, *Journal of Fluid Mechanics*, 135, 337,
510 doi:10.1017/S0022112083003110.
- 511 Ling, B., J. Bao, M. Oostrom, I. Battiato, and A. M. Tartakovsky (2017), Modeling variabil-
512 ity in porescale multiphase flow experiments, *Advances in Water Resources*, 105, 29–38,
513 doi:10.1016/j.advwatres.2017.04.005.
- 514 Liu, Y.-Y., J.-J. Slotine, and A.-L. Barabasi (2013), Observability of complex sys-
515 tems, *Proceedings of the National Academy of Sciences*, 110(7), 2460–2465, doi:
516 10.1073/pnas.1215508110.

- 517 Masalmeh, S. K., X. Jing, S. Roth, C. Wang, H. Dong, and M. Blunt (2015), Towards Pre-
518 dicting Multi-Phase Flow in Porous Media Using Digital Rock Physics : Workflow to Test
519 the Predictive Capability of Pore-Scale Modeling Outline of the Workflow, in *Abu Dhabi*
520 *International Petroleum Exhibition and Conference*, Society of Petroleum Engineers, Abu
521 Dhabi, UAE, doi:10.2118/177572-MS.
- 522 McClure, J. E., R. T. Armstrong, M. A. Berrill, S. Schlüter, S. Berg, W. G. Gray, and C. T.
523 Miller (2018), Geometric state function for two-fluid flow in porous media, *Physical Re-*
524 *view Fluids*, 3(8), 084,306, doi:10.1103/PhysRevFluids.3.084306.
- 525 Meakin, P., and A. M. Tartakovsky (2009), Modeling and simulation of pore-scale multi-
526 phase fluid flow and reactive transport in fractured and porous media, *Reviews of Geo-*
527 *physics*, 47(3), RG3002, doi:10.1029/2008RG000263.
- 528 Øren, P., L. Ruspini, M. Saadatfar, R. Sok, M. Knackstedt, and A. Herring (2019), In-
529 situ pore-scale imaging and image-based modelling of capillary trapping for geologi-
530 cal storage of CO₂, *International Journal of Greenhouse Gas Control*, 87, 34–43, doi:
531 10.1016/j.ijggc.2019.04.017.
- 532 Øren, P.-E., S. Bakke, and O. J. Arntzen (1998), Extending Predictive Capabilities to Net-
533 work Models, *SPE Journal*, 3(04), 324–336, doi:10.2118/52052-PA.
- 534 Raeni, A. Q., B. Bijeljic, and M. J. Blunt (2017), Generalized network modeling: Network
535 extraction as a coarse-scale discretization of the void space of porous media, *Physical Re-*
536 *view E*, 96(1), 013,312, doi:10.1103/PhysRevE.96.013312.
- 537 Reynolds, C. A., H. Menke, M. Andrew, M. J. Blunt, and S. Krevor (2017), Dynamic fluid
538 connectivity during steady-state multiphase flow in a sandstone, *Proceedings of the Na-*
539 *tional Academy of Sciences*, 114(31), 8187–8192, doi:10.1073/pnas.1702834114.
- 540 Rucker, M., S. Berg, R. T. Armstrong, A. Georgiadis, H. Ott, A. Schwing, R. Neiteler,
541 N. Brussee, A. Makurat, L. Leu, M. Wolf, F. Khan, F. Enzmann, and M. Kersten (2015),
542 From connected pathway flow to ganglion dynamics, *Geophysical Research Letters*,
543 42(10), 3888–3894, doi:10.1002/2015GL064007.
- 544 Ruspini, L. C., R. Farokhpoor, and P. E. Øren (2017), Pore-scale modeling of capillary trap-
545 ping in water-wet porous media: A new cooperative pore-body filling model, *Advances in*
546 *Water Resources*, 108, 1–14, doi:10.1016/j.advwatres.2017.07.008.
- 547 Scanziani, A., K. Singh, M. J. Blunt, and A. Guadagnini (2017), Automatic method for es-
548 timation of in situ effective contact angle from X-ray micro tomography images of two-
549 phase flow in porous media, *Journal of Colloid and Interface Science*, 496, 51–59, doi:

550 10.1016/j.jcis.2017.02.005.

551 Schlüter, S., S. Berg, M. Rücker, R. T. Armstrong, H.-J. Vogel, R. Hilfer, and D. Wilden-
552 schild (2016), Pore-scale displacement mechanisms as a source of hysteresis for
553 two-phase flow in porous media, *Water Resources Research*, 52(3), 2194–2205, doi:
554 10.1002/2015WR018254.

555 Schlüter, S., S. Berg, T. Li, H.-J. Vogel, and D. Wildenschild (2017), Time scales of relax-
556 ation dynamics during transient conditions in two-phase flow, *Water Resources Research*,
557 53(6), 4709–4724, doi:10.1002/2016WR019815.

558 Shams, M., A. Q. Raeini, M. J. Blunt, and B. Bijeljic (2018), A numerical model of two-
559 phase flow at the micro-scale using the volume-of-fluid method, *Journal of Computational*
560 *Physics*, 357, 159–182, doi:10.1016/j.jcp.2017.12.027.

561 Singh, K., B. Bijeljic, and M. J. Blunt (2016), Imaging of oil layers, curvature, and contact
562 angle in a mixed-wet and a water-wet carbonate rock, *Water Resources Research*, pp. n/a–
563 n/a, doi:10.1002/2015WR018072.

564 Singh, K., H. Menke, M. Andrew, Q. Lin, C. Rau, M. J. Blunt, and B. Bijeljic (2017), Dy-
565 namics of snap-off and pore-filling events during two-phase fluid flow in permeable media,
566 *Scientific Reports*, 7(1), 5192, doi:10.1038/s41598-017-05204-4.

567 Singh, K., H. Menke, M. Andrew, C. Rau, B. Bijeljic, and M. J. Blunt (2018), Time-resolved
568 synchrotron X-ray micro-tomography datasets of drainage and imbibition in carbonate
569 rocks, *Scientific Data*, 5, 180,265, doi:10.1038/sdata.2018.265.

570 Sorbie, K. S., and A. Skauge (2011), Can network modelling predict two-phase flow func-
571 tions?, in *Int. Symp. Soc. Core Analysts*, 1956, Society of Core Analysts, Austin, USA.

572 Valvatne, P. H., and M. J. Blunt (2004), Predictive pore-scale modeling of two-
573 phase flow in mixed wet media, *Water Resources Research*, 40(7), n/a–n/a, doi:
574 10.1029/2003WR002627.

575 Wildenschild, D., and A. P. Sheppard (2013), X-ray imaging and analysis techniques for
576 quantifying pore-scale structure and processes in subsurface porous medium systems, *Ad-
577 vances in Water Resources*, 51(0), 217–246, doi:10.1016/j.advwatres.2012.07.018.

578 Wilkinson, D., and J. F. Willemsen (1983), Invasion percolation: a new form of percola-
579 tion theory, *Journal of Physics A: Mathematical and General*, 16(14), 3365–3376, doi:
580 10.1088/0305-4470/16/14/028.

581 Youssef, S., H. Deschamps, J. Dautriat, E. Rosenberg, R. Oughanem, E. Maire, and
582 R. Mokso (2013), 4D Imaging of fluid flow dynamics in natural porous media with ultra-

583 fast X-ray microtomography, in *Int. Symp. Soc. Core Analysts*, Society of Core Analysts,
584 Napa Valley, USA.

585 Zhao, B., C. W. MacMinn, and R. Juanes (2016), Wettability control on multiphase flow
586 in patterned microfluidics, *Proceedings of the National Academy of Sciences*, *113*(37),
587 10,251–10,256, doi:10.1073/pnas.1603387113.

588 Zou, S., R. T. Armstrong, J.-y. Arns, C. H. Arns, and F. Hussain (2018), Experimen-
589 tal and Theoretical Evidence for Increased Ganglion Dynamics During Fractional
590 Flow in Mixed-Wet Porous Media, *Water Resources Research*, *54*(5), 3277–3289, doi:
591 10.1029/2017WR022433.